





Cite this: *RSC Adv.*, 2019, 9, 13082

Three new metal coordination polymers of bifunctional imidazolate/tetrazolate bridges: the only example of a three-dimensional framework based on rare $[\text{Co}_4(\mu_3\text{-OH})_2(\mu_2\text{-Cl})_2]^{4+}$ mixed oxo-chloro-clusters†

Lili Yang,^a Jian Zhou,^b  ^{*,a} Hua-Hong Zou  ^{*,b} and Qiuling Tang^a

Three new metal coordination polymers $[\text{Ni}(\mu_2\text{-L})_2(\text{H}_2\text{O})_2]_n$ (**1**, HL = 1-tetrazole-4-imidazole-benzene), $[\text{Co}(\mu_2\text{-L})_2]_n$ (**2**), and $[\text{Co}_4(\mu_3\text{-OH})_2(\mu_2\text{-Cl})_2(\mu_5\text{-L})_2(\mu_2\text{-L})_2]_n \cdot 7n\text{H}_2\text{O}$ (**3**) were hydrothermally synthesized and structurally characterized. **1** displays a neutral $[\text{Ni}(\mu_2\text{-L})_2(\text{H}_2\text{O})_2]_n$ chain built up from the Ni^{2+} ions bridged by deprotonated L^- ligands, while **2** shows another rare neutral $[\text{Co}(\mu_2\text{-L})_2]_n$ chain based on Co^{2+} ions connected by two different coordination modes of the L^- ligand. **3** exhibits a rare $[\text{Co}_4(\mu_3\text{-OH})_2(\mu_2\text{-Cl})_2]^{4+}$ mixed oxo-chloro-cluster-based three-dimensional framework with large elliptical channels, which are filled by unprecedented chilopod $[(\text{H}_2\text{O})_7]_n$ chains. Both **1** and **2** show antiferromagnetic behavior, while **3** exhibits unusual spin-canting.

Received 21st February 2019

Accepted 23rd April 2019

DOI: 10.1039/c9ra01327j

rsc.li/rsc-advances

Introduction

Magnetic metal coordination polymers with varied fascinating architectures associated with rich magnetic character have attracted considerable attention, due to their potential applications in high-density information storage and processing, quantum computing, and molecular spintronics devices.¹ The appropriate bridging ligands between paramagnetic metal ions have a significant effect on the magnetic behaviors *via* transmitting magnetic coupling efficiently. Five-membered heterocyclic polyazoles (such as imidazole,² triazole³ and tetrazole⁴) and their derivatives are excellent candidates for active magnetic bridges, because their various bridging modes can aggregate multiple metal ions into polynuclear clusters and engage in superexchange interactions to offer materials with useful magnetic properties. Among these polyazoles, imidazoles can be efficient heterocyclic bridging ligands for the syntheses of molecule-based magnets, due to the absence of an inversion center along the NCN bridge,² while tetrazoles with

antisymmetric bridging modes can produce antisymmetric superexchange interactions, resulting in spin canting behavior and long-range magnetic ordering.⁴ Expectedly, the coexistence of imidazole and tetrazole in the same organic framework may generate a new class of bifunctional bridging ligands. The representative bifunctional bridge is 1-tetrazole-4-imidazole-benzene (HL) containing one imidazole and one tetrazole, which was used mainly for the construction of luminescent coordination polymers of d^{10} metal ions (such as Cu^+ , Ag^+ , Zn^{2+} and Cd^{2+}) owing to its aromatic chromophore and diverse bridging modes.⁵ However, its magnetic coordination polymers of paramagnetic metal ions (such as $\text{Mn}^{2/3+}$, $\text{Fe}^{2/3+}$, Co^{2+} , and Ni^{2+}) have been less explored, and the limited examples are cobalt(II) coordination polymers $[\text{Co}_2(\text{L})_2(\text{HL})(\text{H}_2\text{O})_2][(\beta\text{-Mo}_8\text{O}_{26})_{0.5}]^{6a}$ and $[\text{Co}_2(\text{L})_2(\text{pbda})\text{-}(\text{H}_2\text{O})_3]$ (H_2pbda = 1,4-benzene-dicarboxylic acid),^{6b} which all show antiferromagnetic behavior, but other important magnetic behaviors have not been documented.

Moreover, the bifunctional bridged ligands containing imidazole and tetrazole groups coordinate to the iron group metal ions to usually generate a variety of metal coordination polymers with octahedrally coordinated metal centers,^{5,6} but their magnetic metal coordination polymers with tetrahedrally coordinated metal centers have not been to date documented, because of synthetic difficulties. The low coordination number of the metal complexes with tetrahedrally coordinated metal centers splitting the d orbitals with a small separation is preferable to form a weak ligand field, which might facilitate the spin-orbital coupling to enhance the magnetic anisotropy, thus resulting in slow magnetic relaxation.⁷ It is expected that the

^aChongqing Key Laboratory of Inorganic Functional Materials, College of Chemistry, Chongqing Normal University, Chongqing 401331, P. R. China. E-mail: Jianzhou88888@163.com

^bState Key Laboratory for Chemistry and Molecular Engineering of Medicinal Resources, School of Chemistry & Pharmacy of Guangxi Normal University, Guilin 541004, P. R. China. E-mail: gxnuchem@foxmail.com

† Electronic supplementary information (ESI) available: Crystal data in CIF format, XRD data, the magnetization *versus* the dc field in the temperature range of 2–5 K for **3**, and some figures. CCDC 1892465 (**1**), 1892466 (**2**) and 1865774 (**3**). For ESI and crystallographic data in CIF or other electronic format see DOI: 10.1039/c9ra01327j



combination of the magnetic metal ions with tetrahedrally coordinated metal centers and the bifunctional imidazole/tetrazole bridges in the same coordination polymeric frameworks may give a new class of coordination polymers with novel structures and useful magnetic properties. With regard to all aspects stated above, we chose HL as magnetic active bridge, and $\text{Co}^{2+}/\text{Ni}^{2+}$ ions as the paramagnetic centre based on the listed below considerations: (a) HL containing two types of heterocyclic polyazoles can not only act as a various magnetic bridges to offer varied architectures and superexchange capacity that might produce significant magnetic properties, but also serve as a diamagnetic separator, owing to tetrazole and imidazole rings separated by benzene ring. (b) Co^{2+} and Ni^{2+} ions are selected as the paramagnetic metal ions that could result in unusual magnetic behaviors.^{4,8} As a result, three new coordination polymers $[\text{Ni}(\mu_2\text{-L})_2(\text{H}_2\text{O})_2]_n$ (**1**), $[\text{Co}(\mu_2\text{-L})_2]_n$ (**2**), $[\text{Co}_4(\mu_3\text{-OH})_2(\mu_2\text{-Cl})_2(\mu_5\text{-L})_2(\mu_2\text{-L})_2]_n \cdot 7n\text{H}_2\text{O}$ (**3**) were obtained by hydrothermal methods. **1** shows the $[\text{Ni}(\mu_2\text{-L})_2(\text{H}_2\text{O})_2]_n$ chain with six-coordinate Ni^{2+} center, while **2** exhibits another rare $[\text{Co}(\mu_2\text{-L})_2]_n$ chain based on four-coordinate Co^{2+} centres. **3** offers the only example of three-dimensional framework incorporating rare mixed oxo-chloro-clusters $[\text{Co}_4(\mu_3\text{-OH})_2(\mu_2\text{-Cl})_2]^{4+}$, mainly because the reported magnetic $[\text{M}_x\text{Q}_y]$ ($\text{Q} = \text{-OH}$ or halogen element) clusters bonding directly to either tetrazole or its derivatives contain only one type of bridge, such as $[\text{Cu}_3(\mu_3\text{-OH})]^{5+}$ ($\text{M} = \text{Mn}, \text{Co}, \text{Cu}$),⁹ $[\text{M}_4(\mu_3\text{-OH})_2]^{6+}$ ($\text{M} = \text{Mn}, \text{Co}$),¹⁰ $[\text{Co}_4(\mu_3\text{-Cl})]^{7+}$,¹¹ and $[\text{Co}_5(\mu_3\text{-F})_2]^{8+}$,^{10a} but the coexistence of -OH and halogen bridges in the same magnetic clusters is only observed in $[\text{Co}_4(\mu_3\text{-OH})_2(\mu_2\text{-Cl})_2]^{4+}$ cluster of **3**.

Experimental

General remarks

All reagents in the preparation procedure were of analytical reagent grade and used without any purification or degassing of solvents. Elemental analyses (C and H) were performed using a PE2400 II elemental analyzer. FT-IR spectra were recorded with a Nicolet Magna-IR 550 spectrometer in dry KBr disks in the 4000–400 cm^{-1} range. The solid-state UV/Vis spectra were measured at room temperature using a PE Lambda 900 UV/Vis spectrophotometer. Powder X-ray diffraction (XRD) patterns were recorded in the angular range of $2\theta = 5\text{--}60^\circ$ on a Bruker D8 advance diffractometer using $\text{CuK}\alpha$ radiation. All magnetization of compounds **1–3** were obtained with a Quantum Design MPMS-XL-5 magnetometer.

Synthesis of $[\text{Ni}(\mu_2\text{-L})_2(\text{H}_2\text{O})_2]_n$ (1**).** The reactants of H_3BO_3 (0.1014 g, 1.6 mmol), NiCl_2 (0.0899 g, 0.7 mmol), HL (0.0256 g, 0.12 mmol) was stirred for 0.5 h, and then the final mixture was sealed in a 25 mL Teflon lined autoclave. The reaction was heated at 170 °C for 7 days. After cooling to room temperature slowly, orange sheet crystals of **1** in about 51% (based on HL) were obtained. Anal calc. (found %) for $\text{C}_{20}\text{H}_{18}\text{N}_{12}\text{NiO}_2$ (**1**): C 46.45 (46.53), H 3.51 (3.59), N 32.50 (32.61). IR (KBr, cm^{-1}): 3420(m), 3096(m), 1543(m), 1515(s), 1440(m), 1311(m), 1255(m), 1117(w), 1079(m), 960(m), 849(s), 747(m), 655(m), 535(m).

Synthesis of $[\text{Co}(\mu_2\text{-L})_2]_n$ (2**).** The reactants of H_3BO_3 (0.1082 g, 1.7 mmol), CoCl_2 (0.0313 g, 0.24 mmol), HL (0.0253 g, 0.12 mmol) and H_2O (2.0 mL) was stirred for 0.5 h, and then the final mixture was sealed in a 25 mL Teflon lined autoclave. The reaction was heated at 170 °C for 7 days. After cooling to room temperature slowly, purple block crystals of **2** in about 43% (based on HL) were obtained. Anal calc. (found %) for $\text{C}_{20}\text{H}_{14}\text{CoN}_{12}$ (**2**): C 49.91 (49.96), H 2.93 (2.98), N 34.92 (34.97). IR (KBr, cm^{-1}): 3135(s), 1612(m), 1546(m), 1511(s), 1443(s), 1368(m), 1309(s), 1105(m), 1065(s), 954(m), 845(s), 758(m), 649(s), 534(m).

Synthesis of $[\text{Co}_4(\mu_3\text{-OH})_2(\mu_2\text{-Cl})_2(\mu_5\text{-L})_2(\mu_2\text{-L})_2]_n \cdot 7n\text{H}_2\text{O}$ (3**).** The reactants of H_3BO_3 (0.1093 g, 1.8 mmol), CoCl_2 (0.0651 g, 0.5 mmol), HL (0.0266 g, 0.13 mmol) and H_2O (2.0 mL) was stirred for 0.5 h, and then the final mixture was sealed in a 25 mL Teflon lined autoclave. The reaction was heated at 170 °C for 7 days. After cooling to room temperature slowly, red needle-like crystals of **3** in about 63% (based on HL) were obtained. Anal calc. (found %) for $\text{C}_{40}\text{H}_{44}\text{Cl}_2\text{Co}_4\text{N}_{24}\text{O}_9$ (**3**): C 36.63 (36.70), H 3.38 (3.43), N 25.63 (25.71). IR (KBr, cm^{-1}): 3619(m), 3453(m), 3131(s), 1608(s), 1499(vs), 1442(vs), 1363(m), 1284(vs), 1128(w), 1060(s), 825(s), 746(m), 650(m), 561(w), 484(w).

X-ray crystallography

Diffraction intensity data for **1–3** were recorded on a Rigaku Mercury CCD diffractometer using a ω -scan method with graphite monochromated $\text{Mo K}\alpha$ radiation ($\lambda = 0.71073 \text{ \AA}$). Absorption corrections were applied using multi-scan technique. The structures of **1–3** were solved by direct methods (SHELXS-97)¹² and refined by full-matrix least-squares techniques using the SHELXL-97 program.¹³ All non-H atoms were refined anisotropically. The H atoms of L^{-1} ligands were added geometrically and refined as riding on their parent atoms with fixed isotropic displacement parameters. Relevant crystal collection data parameters and refinement results can be found in Table 1. CCDC numbers are 1892465 (**1**), 1892466 (**2**) and 1865774 (**3**).

Results and discussion

Synthetic aspects

The crystals of **1–3** were obtained by the reaction of MCl_2 ($\text{M} = \text{Co}, \text{Ni}$), H_3BO_3 and HL in water solution at 170 °C. Although H_3BO_3 is not introduced into the final structure, numerous paralleling experiments affirmed that **1–3** cannot be obtained in the absence of H_3BO_3 , showing that the H_3BO_3 may take a role as structural directing agent. The parallel experiments reveal that the reactant stoichiometry and initial reactants can influence the outcome of reaction. For instance, when the quantity of CoCl_2 was increased to two times under the similar synthetic procedure to **2**, red crystals of **3** containing mixed oxo-chloro-clusters $[\text{Co}_4(\mu_3\text{-OH})_2(\mu_2\text{-Cl})_2]^{4+}$ were isolated. With the aim of preparing an analogue of **3**, we tried to replace CoCl_2 with NiCl_2 alone, but these attempts failed and orange crystal of **1** was the only pure product isolated. The IR spectra of **1** and **3** show the several strong absorptions in the range of 3420–3619 cm^{-1} ,

indicative of the characteristic ν_{OH} vibration of $-\text{OH}$ groups and H_2O molecules, but no similar ν_{OH} vibration is observed in **2**. The peak at 3131 cm^{-1} can be assigned to $\nu_{\text{C-H}}$ stretching, while the several bands in the range of $1284\text{--}1612\text{ cm}^{-1}$ are attributed to the characteristic $\nu_{\text{C-N}}$, $\nu_{\text{C=C}}$ and $\nu_{\text{N=N}}$ vibrations of the L^- ligand. The phase purities of **1**–**3** are confirmed by PXRD analysis (Fig. S1†).

Description of the structure

Description of $[\text{Ni}(\mu_2\text{-L})_2(\text{H}_2\text{O})_2]_n$ (1**) and $[\text{Co}(\mu_2\text{-L})_2]_n$ (**2**).** **1** crystallizes in triclinic space group $P\bar{1}$ and its asymmetric unit contains one unique L^- ligand, one coordinated H_2O , and half of a Ni^{2+} ion located at the special position with 2-fold symmetry (Fig. S2a†). The Ni^{2+} ion is octahedrally coordinated to four N atoms from four L^- ligands and two H_2O molecules. The Ni–O and Ni–N bond lengths are normal and call for no further comment.¹⁴ The neighboring complex $[\text{Ni}(\text{H}_2\text{O})_2]^{2+}$ cations are bridged by double L^- ligands to give a chain $[\text{Ni}(\mu_2\text{-L})_2(\text{H}_2\text{O})_2]_n$ (Fig. 1a) with a Ni \cdots Ni distance of 10.98 Å.

2 crystallizes in monoclinic space group $C2/c$. The asymmetric unit contains one unique Co^{2+} ions and two L^- ligands (Fig. S2b†). Each Co^{2+} ion adopts a tetrahedral coordination mode comprised of four N atoms from four L^- ligands. The Co–N bond lengths are in the range of 1.995(3)–2.018(3) Å, comparable to corresponding values (1.855(5)–2.155(4) Å) in other compounds.^{7c} The L^- ligand shows two different bridging modes, namely, $\mu_2\text{-}\kappa\text{N1}:\kappa\text{N3}$ and $\mu_2\text{-}\kappa\text{N7}:\kappa\text{N12}$. The neighboring Co^{2+} ions are bridged by $\mu_2\text{-}\kappa\text{N1}:\kappa\text{N3}$ bridging ligand to form a $[\text{Co}_2\text{L}_2]$ dimer with a Co \cdots Co distance of 10.54 Å. The $[\text{Co}_2\text{L}_2]$ dimer units are interconnected *via* $\mu_2\text{-}\kappa\text{N7}:\kappa\text{N12}$ bridging ligand to form a chain $[\text{Co}(\mu_2\text{-L})_2]_n$ with elliptical ring (Fig. 1b).

Description of $[\text{Co}_4(\mu_3\text{-OH})_2(\mu_2\text{-Cl})_2(\mu_5\text{-L})_2(\mu_2\text{-L})_2]_n \cdot 7n\text{H}_2\text{O}$ (3**).** **3** crystallizes in monoclinic space group $C2/c$ and its asymmetric unit contains two Co^{2+} ions, two L^- ligands, one Cl^- anion, one $-\text{OH}$ group, three and half of H_2O , where O3W atom is seated at the special position with 2-fold symmetry (Fig. 2a).

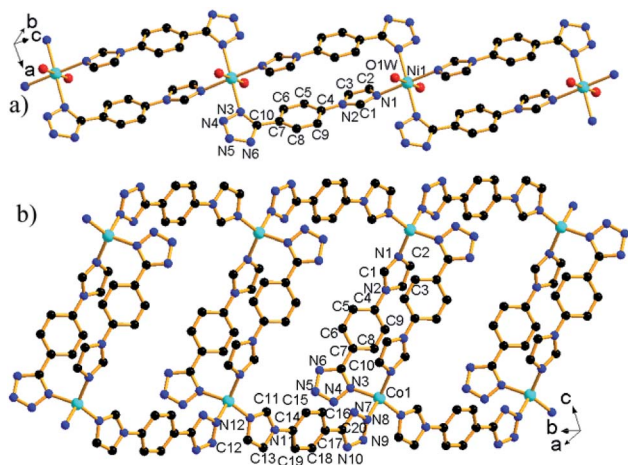


Fig. 1 The structures of $[\text{Ni}(\mu_2\text{-L})_2(\text{H}_2\text{O})_2]_n$ (a) and $[\text{Co}(\mu_2\text{-L})_2]_n$ (b) chains. All H atoms bonded to C and O atoms have been omitted for clarity.

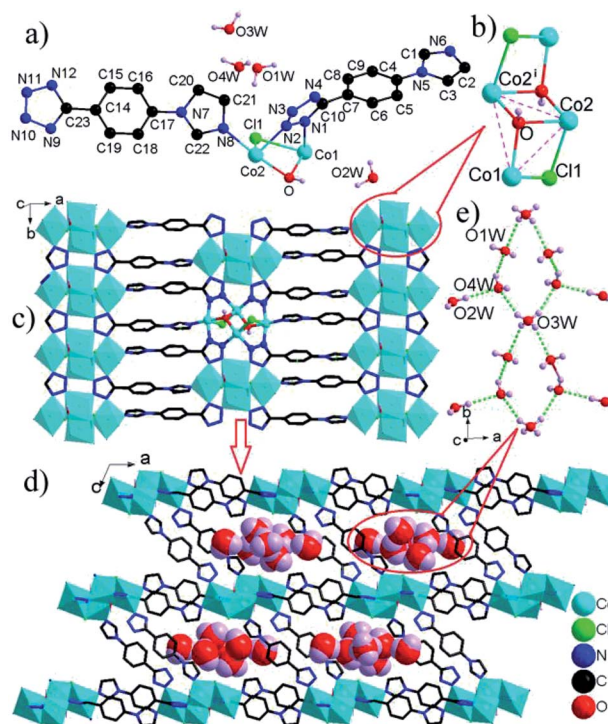


Fig. 2 (a) The asymmetric unit of **3** with labeling scheme. (b) $[\text{Co}_4(\mu_3\text{-OH})_2(\mu_2\text{-Cl})_2]^{4+}$ mixed oxo-chloro-cluster [symmetry operation: (i) $-x, -y, 1-z$]. (c) The layer built from $[\text{Co}_4(\mu_3\text{-OH})_2(\mu_2\text{-Cl})_2]^{4+}$ clusters and L^- ligands. (d) Three-dimensional framework of **3**. (e) chilopod $[(\text{H}_2\text{O})_7]_n$ chain. H atoms bonded to C atoms are omitted for clarity.

$\text{Co}(1)^{2+}$ ion adopts an octahedral coordination environment comprised of four N atoms from four different L^- ligands, one $\mu_2\text{-Cl}^-$ ion and one $\mu_3\text{-OH}$ group, while $\text{Co}(2)^{2+}$ ion has a similar octahedron ligated by three N atoms from three different L^- ligands, one $\mu_2\text{-Cl}^-$ ion and two $\mu_3\text{-OH}$ groups. The Co–N/O bond lengths are in the range of 2.056(3)–2.206(4) Å, and the Co–Cl bond lengths vary from 2.5232(12) to 2.5251(12) Å, which are compared with corresponding bond lengths (2.032(2)–2.206(2) Å for Co–N/O and 2.428(1)–2.7019(7) Å for Co–Cl) in

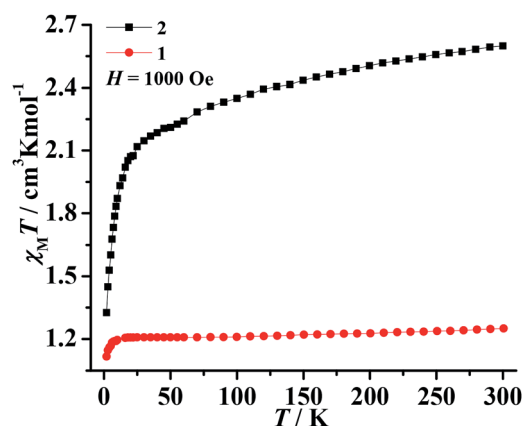


Fig. 3 Temperature dependence of the $\chi_M T$ product for **1**–**2** at 1000 Oe.

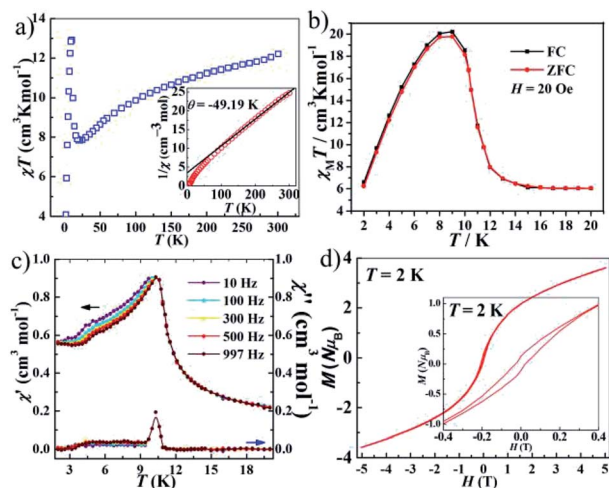


Fig. 4 (a) The temperature dependence of $\chi_m T$ under $H_{dc} = 1000$ Oe between 2 and 300 K (inset: fitting C and θ of $1/\chi$ for **3**). (b) ZFC and FC curves at 20 Oe. (c) The temperature dependence of the in-phase (χ') and out-of-phase (χ'') ac-susceptibilities for different frequencies in zero dc-field for **3**. (d) The isothermal field dependence of magnetization at 2 K.

other compounds.^{14,15} There are two bridging modes of L^- ligand (denoted as L1 and L2, Fig. S3†) in **3**. The L1 ligand shows a $\mu_5\text{-}\kappa\text{N1}:\kappa\text{N2}:\kappa\text{N3}:\kappa\text{N4}:\kappa\text{N6}$ bridging mode, while the L2 ligand exhibits a $\mu_2\text{-}\kappa\text{N8}:\kappa\text{N11}$ bridging mode. All atoms in L1 and L2 are not coplanar, mainly because the dihedral angle of benzene ring and imidazole ring is 8.19° for L1 and 26.54° for L2, and the dihedral angle of benzene ring and tetrazole ring is 65.31° for L1 and 8.29° for L2. Four Co^{2+} ions are bridged by two $\mu_3\text{-OH}$ groups and two $\mu_2\text{-Cl}^-$ ions to form a novel tetra-nuclear

$[\text{Co}_4(\mu_3\text{-OH})_2(\mu_2\text{-Cl})_2]^{4+}$ mixed oxo-chloro-cluster with Co...Co distances of 3.127–3.596 Å (Fig. 2b). This cluster might be also viewed as a derivative of the butterfly-shaped $[\text{Co}_4(\mu_3\text{-OH})_2]$ cluster, whose Co^{2+} ions are further bridged by two $\mu_2\text{-Cl}^-$ ions.

The $[\text{Co}_4(\mu_3\text{-OH})_2(\mu_2\text{-Cl})_2]^{4+}$ clusters are interconnected by L1 ligands to form an infinite $[\text{Co}_4(\mu_3\text{-OH})_2(\mu_2\text{-Cl})_2]^{4+}$ cluster-based 2-D layer (Fig. 2c). The nearest Co...Co distance between adjacent clusters spanned by tetrazole ring of L^- ligand is much shorter than that by whole L^- connector (4.21 versus 10.43 Å), resulting in the significant superexchange interactions within the Co-tetrazole ribbon. These layers are further bridged by L2 ligands to generate a three-dimensional network structure with large elliptical channels filled by $[(\text{H}_2\text{O})_7]_n$ chilopod chains (Fig. 2d). The free H_2O molecules are interconnected *via* O-H...O H-bonds to form chilopod $[(\text{H}_2\text{O})_7]_n$ chain (Fig. 2e), which contains cyclic hexamer $(\text{H}_2\text{O})_6$ with a pseudo-crown conformation (Fig. S4†) and $\text{H}_2\text{O}(2\text{W})$ foot. The average O...O distance of 2.894 Å is close to the corresponding value (2.85 Å) in liquid H_2O .¹⁶ So far, some infinite cyclic water chains have been reported, as exemplified by T4(1), T4(1)6(1), T4(2)6(2), T5(2), T6(1) and T6(2) modes,¹⁷ but their cyclic chains decorated by branch-like H_2O molecules are very rare.¹⁸ The $[(\text{H}_2\text{O})_7]_n$ chain in **3** can be regarded as T6(1) chain decorated by one branch-like H_2O molecule, which exhibits a new type of cyclic water chain. Notably, some metal coordination polymers of L^- ligands have been reported, but no water chains are observed within their extended architectures.^{5,6} Therefore, **3** offers the only example of three-dimensional architecture based on L^- ligands with channels filled by chilopod $[(\text{H}_2\text{O})_7]_n$ chains.

More interestingly, some three-dimensional extended frameworks are built up from the linkages of metal ions and a mixed bridge of L^- ligand and aromatic carboxylate to date,^{5b-g} but similar three-dimensional architectures containing only

Table 1 Crystallographic data for 1–3

	1	2	3
Formula	$\text{C}_{20}\text{H}_{18}\text{N}_{12}\text{NiO}_2$	$\text{C}_{20}\text{H}_{14}\text{CoN}_{12}$	$\text{C}_{40}\text{H}_{44}\text{Cl}_2\text{Co}_4\text{N}_{24}\text{O}_9$
Fw	517.15	481.36	1311.61
Crystal system	Triclinic	Monoclinic	Monoclinic
Space group	$P\bar{1}$	$C2/c$	$C2/c$
a , Å	7.4760(8)	9.3788(6)	32.117(4)
b , Å	7.9402(7)	12.9170(7)	6.5151(8)
c , Å	9.3241(10)	31.877(2)	25.559(3)
α , °	102.237(3)	90	90
β , °	98.119(4)	95.654(2)	113.333(3)
γ , °	106.700(3)	90	90
V , Å ³	505.87(9)	3843.0(4)	4910.6(10)
Z	1	8	4
T , K	289(2)	296(2)	296(2)
Calcd density, mg m^{-3}	1.698	1.664	1.774
$F(000)$	266	1960	2664
2θ (max), deg	50.18	50.20	50.20
Total reflns collected	4031	14 381	16 564
Unique reflns	1755	3380	4364
No. of param	168	298	359
$R_1[I > 2\sigma(I)]$	0.0581	0.0317	0.0471
$wR2$ (all data)	0.1468	0.0779	0.1387
GOOF on F^2	1.076	1.060	1.057

one type of L^- ligand are relatively scarce, and the limited examples include $[Cu_2(\mu_4-L)_2]_n$ with 4-connected $SrAl_2$ topology constructed by simple Cu^+ ions and μ_4-L bridges,^{5b} and $[Cu_2-Cl(\mu_5-L)]_n$ with bimodal fsc-3,5-Cmce-2 topology based on the combination of L^- ligands and dimeric $[Cu_2Cl]^+$ cluster units,^{5f} in which the number of metal ions within the cluster unit is not more than two, but the number of Co^{2+} ions in the $[Co_4(\mu_3-OH)_2(\mu_2-Cl)_2]^{4+}$ cluster of **3** is four. Hence, **3** is the only example of 3-D framework based on the linkages of high-nuclear magnetic $[Co_4(\mu_3-OH)_2(\mu_2-Cl)_2]^{4+}$ clusters and L^- ligands.

Magnetic properties

The magnetic susceptibilities of polycrystalline samples of **1–3** were measured on cooling from 300 to 2 K in an applied field of 1000 Oe. The values of $\chi_M T$ at 300 K are $1.25 \text{ cm}^3 \text{ K mol}^{-1}$ for **1** and $2.59 \text{ cm}^3 \text{ K mol}^{-1}$ for **2** (Fig. 3), which are higher than the spin-only value for one isolated Ni^{2+} ion ($1.0 \text{ cm}^3 \text{ K mol}^{-1}$, $S = 1$) and Co^{2+} ion ($1.875 \text{ cm}^3 \text{ K mol}^{-1}$, $S = 3/2$). This phenomenon in **2** is very common for Co^{2+} due to the significant orbital contribution,¹⁹ and it in **1** could result from the orbital contribution of the $^3A_{2g}$ ground state of the high-spin octahedrally coordinated Ni^{2+} ion.²⁰ The values of $\chi_M T$ slowly decrease upon decreasing temperature and the $\chi_M T$ values are $1.21 \text{ cm}^3 \text{ K mol}^{-1}$ for **1** (at 20 K) and $2.23 \text{ cm}^3 \text{ K mol}^{-1}$ for **2** (at 70 K). On further cooling, another sharply decreases of $\chi_M T$ are observed, to $0.52 \text{ cm}^3 \text{ K mol}^{-1}$ for **1** and $1.31 \text{ cm}^3 \text{ K mol}^{-1}$ for **2** at 2 K. The plots are indicative of typical antiferromagnetic interactions between the adjacent M^{2+} ions ($M = Ni^{2+}$ and Co^{2+}). In order to assess the possible dynamics of magnetization, ac susceptibility measurements were performed under zero dc field and 2.5 Oe ac field oscillating at different frequency (Fig. S5†). However, the results show a complete absence of an out-of-phase component above 2 K.

The value of $\chi_M T$ at 300 K was $12.20 \text{ cm}^3 \text{ K mol}^{-1}$ for **3**, upon cooling, $\chi_M T$ decreases quickly up to *ca.* 20 K before going through minima around 20 K, then rises rapidly to a sharp maximum at 10 K, and finally drops rapidly due to saturation effects (Fig. 4a). The phenomenon is reminiscent of ferromagnetic behavior. Analyses of the χ_M^{-1} vs. T data above 150 K using the Curie–Weiss law give estimated Curie constants were $14.01 \text{ cm}^3 \text{ K mol}^{-1}$ and Weiss constants (θ) were -49.19 K for **3**. The Curie constants are normal for octahedrally coordinated Co^{2+} and the negative Weiss constants indicate intracluster antiferromagnetic coupling above 150 K. The negative value of θ and the initial decrease of $\chi_M T$ should be due to the synergistic effect of spin–orbital coupling of Co^{2+} and the antiferromagnetic coupling through the tetrazolate bridge. The ferrimagnetic behavior has been confirmed by the ZFC–FC magnetization measurements 20 Oe (Fig. 4b). The curve exhibit small differences and both have a sharp maximum at *ca.* 10 K, suggesting the occurrence of interlayer antiferromagnetic ordering below $T_N = 10 \text{ K}$ and a canting angle of about 0.37° . The χ_M versus T data at different fields (100–5000 Oe) (Fig. S6†) reveal that an abrupt increase of χ_M values below about 10 K is influenced by increasing the applied field, which becomes insignificant until almost invisible at about 5000 Oe, owing to the saturation

effects. For the alternating current (ac) susceptibilities at different frequencies (Fig. 4c), a sharp peak was observed at *ca.* 10 K in both the real and imaginary components, further confirming the long-range ordering of spin-canted antiferromagnetic in **3** and coinciding with the T_N obtained in ZFC/FC measurements. The spin canting may be caused by the anti-symmetric exchange interaction between the Co^{2+} ions in the chain, as well as the single-ion magnetic anisotropy of Co^{2+} . The isothermal magnetization of **3** was measured at 2–5 K as a function of applied magnetic field up to 5 T following cooling in zero field (Fig. S7†). The value reaching $3.64 \text{ N}\beta$ is lower to that expected for corresponding theoretical value assuming $12 \text{ N}\beta$ per Co_4 unit at 5 T, also confirming the ferrimagnetic behavior. As shown in Fig. 4d, the isothermal magnetization displays an obvious hysteresis loop with a relatively large coercive field and remnant magnetization at 2 K.

Conclusions

Although a few low-dimensional magnetic metal coordination polymers of bifunctional bridges containing imidazolate and tetrazolate groups have been reported to date, they generally exhibits antiferromagnetic behavior. **3** not only presents the only example of three-dimensional framework based on the linkages of rare $[Co_4(\mu_3-OH)_2(\mu_2-Cl)_2]^{4+}$ mixed oxo-chloro-clusters and bifunctional imidazolate/tetrazolate bridges, but also show unusual spin-canting. Furthermore, the similar bifunctional imidazolate/tetrazolate bridges coordinate to the magnetic metal ions to often form varied metal coordination polymers with octahedrally coordinated metal centers, but **2** is the only example of the magnetic tetrahedral metal coordination polymer with tetrahedrally coordinated metal centers of bifunctional imidazolate/tetrazolate bridges. These results enrich structural types of magnetic metal coordination polymers of bifunctional imidazolate/tetrazolate bridges, and offer possibilities to prepare other novel metal coordination polymers with important magnetic behavior using paramagnetic metal ions in combination with other bifunctional imidazolate/tetrazolate bridges.

Conflicts of interest

There are no conflicts to declare.

Acknowledgements

This work was supported by the NNSF of China (No. 21671029 and 21601038), the NSF of Chongqing (No. cstc2015jcyjBX0117 and cstc2018jcyjAX0157), Program for leading talents of scientific and technological innovation in Chongqing (No. CSTCCXLJRC201707), the innovation Program for Chongqing's overseas Returnees (No. cx2018008), and Program for Excellent Talents in Chongqing Higher Education Institutions. The authors are also grateful to Chongqing Normal University for financial support (No. 14CSLJ02, 13XLZ07).

Notes and references

- 1 (a) S. Hill, R. S. Edwards, N. Aliaga-Alcalde and G. Christou, *Science*, 2003, **302**, 1015–1018; (b) M. N. Leuenerger and D. Loss, *Nature*, 2001, **410**, 789–793; (c) L. Bogani and W. Wernsdorfer, *Nat. Mater.*, 2008, **7**, 179–186; (d) E. Saitoh, H. Miyajima, T. Yamaoka and G. Tatara, *Nature*, 2004, **432**, 203–206; (e) M. Yamanouchi, D. Chiba, F. Matsukura and H. Ohno, *Nature*, 2004, **428**, 539–542.
- 2 (a) J. López-Cabrelles, M. Giménez-Marqués, G. M. Espallargas and E. Coronado, *Inorg. Chem.*, 2015, **54**, 10490–10496; (b) T. C. Stamatatos, S. P. Perlepes, C. P. Raptopoulou, A. Terzis, C. S. Patrickios, A. J. Tasiopoulos and A. K. Boudalis, *Dalton Trans.*, 2009, 3354–3362.
- 3 (a) R. Gautier and R. Clérac, *Cryst. Growth Des.*, 2017, **17**, 864–869; (b) M. M. Dîrtu, A. D. Naik, A. Rotaru, L. Spinu, D. Poelman and Y. Garcia, *Inorg. Chem.*, 2016, **55**, 4278–4295.
- 4 (a) F. Yang, B. Li, W. Xu, G. Li, Q. Zhou, J. Hua, Z. Shi and S. Feng, *Inorg. Chem.*, 2012, **51**, 6813–6820; (b) E. Yang, Z. Liu, T. Liu, L. Li and X. Zhao, *Dalton Trans.*, 2011, **40**, 8132–8813.
- 5 (a) Z. Shi, J. Peng, X. Yu, Z. Zhang, X. Wang and W. Zhou, *Inorg. Chem. Commun.*, 2014, **41**, 8–87; (b) J. Sun, D. Zhang, L. Wang, R. Zhang, J. Wang, Y. Zeng, J. Zhan, J. Xu and Y. Fan, *J. Solid State Chem.*, 2013, **206**, 286–292; (c) S. Hou, J. Tan, Z. Lian, D. Zeng, T. Huang, B. Huang, S. Zheng, J. Fan and W. Zhang, *Inorg. Chem. Commun.*, 2014, **47**, 112–118; (d) Z. Shi, J. Peng, Z. Zhang, X. Yu, K. Alimaje and X. Wang, *Inorg. Chem. Commun.*, 2013, **33**, 105–108; (e) S. Zheng, L. Zhang, J. He, J. Fan and W. Zhang, *Inorg. Chem. Commun.*, 2016, **66**, 19–23; (f) Y. Xie, J. He, T. Wang and H. Zeng, *J. Coord. Chem.*, 2015, **68**, 1733–1742; (g) X. Hu, C. Qin, L. Zhao, F. Liu, K. Shao and Z. Su, *RSC Adv.*, 2015, **5**, 49606–49613; (h) D. Ma, L. Qin, K. Lu, H. Guo and J. Liu, *Inorg. Chem. Commun.*, 2012, **24**, 87–90; (i) Q. Tang, J. Zhou, F. A. Almeida Paz, L. Fu, H. Xiao, Q. Zhou and J. Li, *Dalton Trans.*, 2017, **46**, 1372–1376; (j) L. Wang, W. Yang, W. Zhu, X. Guan, Z. Xie and Z. Sun, *Inorg. Chem.*, 2014, **53**, 11584–11588; (k) J. Chen, Q. Zhang, Z. Liu, S. Wang, Y. Xiao, R. Li, J. Xu, Y. Zhao, F. Zheng and G. Guo, *Dalton Trans.*, 2015, **44**, 10089–10096.
- 6 (a) X. Li, Y. Chen, X. Chi, Y. Xu, Q. Yang, H. Zhang, J. Zhang and D. Xiao, *Inorg. Chim. Acta*, 2015, **437**, 159–166; (b) H. Kuai, X. Cheng and X. Zhu, *Inorg. Chem. Commun.*, 2012, **25**, 43–47.
- 7 (a) J. M. Zadrozny and J. R. Long, *J. Am. Chem. Soc.*, 2011, **133**, 20732–20734; (b) F. Yang, Q. Zhou, Y. Zhang, G. Zeng, G. Li, Z. Shi, B. Wang and S. Feng, *Chem. Commun.*, 2013, **49**, 5289–5291; (c) J. Palion-Gazda, B. Machura, R. Kruszynski, T. Grancha, N. Moliner, F. Lloret and M. Julve, *Inorg. Chem.*, 2017, **56**, 6281–6296.
- 8 (a) S. Hu, L. Yun, Y. Zheng, Y. Lan, A. K. Powell and M. Tong, *Dalton Trans.*, 2009, 1897–1900; (b) X. Li, G. Zhuang, X. Wang, K. Wang and E. Gao, *Chem. Commun.*, 2013, **49**, 1814–1816.
- 9 (a) Y. Chen, Y. Song, Y. Zhang and J. Lang, *Inorg. Chem. Commun.*, 2008, **11**, 572–575; (b) K. Darling, W. Ouellette, A. Prosvirin, S. Freund, K. R. Dunbar and J. Zubieta, *Cryst. Growth Des.*, 2012, **12**, 2662–2672; (c) M. Li, G. Yang, S. Li, H. Zang, G. Xu, K. Shao and Z. Su, *Inorg. Chem. Commun.*, 2010, **13**, 1203–1206.
- 10 (a) W. Ouellette and K. Darling, *Dalton Trans.*, 2011, **40**, 12288–12300; (b) E. Yang, Z. Liu, X. Wu, H. Chang, E. Wang and X. Zhao, *Dalton Trans.*, 2011, **40**, 10082–10089.
- 11 K. Xiong, F. Jiang, Y. Gai, Z. He, D. Yuan, L. Chen, K. Su and M. Hong, *Cryst. Growth Des.*, 2012, **12**, 3335–3341.
- 12 G. M. Sheldrick, *Shelxs-97, Program for the Solution of Crystal Structures*, University of Göttingen, Göttingen (Germany) 1997.
- 13 G. M. Sheldrick, *Shelxl-97, Program for the Refinement of Crystal Structures*, University of Göttingen, Göttingen (Germany) 1997.
- 14 S. Karmakar and S. Khanra, *CrystEngComm*, 2014, **16**, 2371–2383.
- 15 P. Grosshans, A. Jouaiti, M. W. Hosseini and N. Kyritsakas, *New J. Chem.*, 2003, **27**, 793–797.
- 16 A. H. Narten, W. E. Thiessen and L. Blum, *Science*, 1982, **217**, 1033–1034.
- 17 (a) L. Infantes, J. Chisholm and S. Motherwell, *CrystEngComm*, 2003, **5**, 480–486; (b) S. M. Hammer, R. Panisch, M. Kobus, J. Glinemann and M. U. Schmidt, *CrystEngComm*, 2009, **11**, 1291–1302; (c) L. Infantes and S. Motherwell, *CrystEngComm*, 2002, **4**, 454–461.
- 18 S. R. Choudhury, A. D. Jana, E. Colacio, H. M. Lee, G. Mostafa and S. Mukhopadhyay, *Cryst. Growth Des.*, 2007, **7**, 212–214.
- 19 (a) D. Cao, J. Feng, M. Ren, Y. Gu, Y. Song and M. D. Ward, *Chem. Commun.*, 2013, **49**, 8863–8865; (b) M. Murrie, *Chem. Soc. Rev.*, 2010, **39**, 1986–1995.
- 20 (a) O. Oms, A. Dolbecq and P. Mialane, *Chem. Soc. Rev.*, 2012, **41**, 7497–7536; (b) Y.-J. Sun, Q.-Q. Huang, T. Tano and S. Itoh, *Inorg. Chem.*, 2013, **52**, 10936–10948.